# Modelling mass transport through a porous partition: Effect of pore size distribution

**Mohamed Khayet**[*], **Armando Velázquez and Juan I. Mengual**
Department of Applied Physics I, Faculty of Physics, University Complutense of Madrid, Madrid, Spain

[*] Corresponding author
Department of Applied Physics I, Faculty of Physics, University Complutense of Madrid, Avda. Complutense s/n, 28040, Madrid, Spain
Tel.: 34 (91) 394 4454
Fax: 34 (91) 394 5191
E-mail: khayetm@fis.ucm.es

## Abstract

Direct contact membrane distillation process has been studied using microporous polytetrafluoroethylene and polyvinylidene fluoride membranes. The membranes were characterized in terms of their non-wettability, pore size distribution and porosity. The mean pore sizes and pore size distributions were obtained by means of wet/dry flow method. The mean pore size and the effective porosity of the membranes were also determined from the gas permeation test. A theoretical model that considers the pore size distribution together with the gas transport mechanisms through the membrane pores was developed for this process. The contribution of each mass transport mechanism was analyzed. It was found that both membranes have pore size distributions in the Knudsen region and in the transition between Knudsen and ordinary diffusion region. The transition region was the major contribution to mass transport. The predicted water vapor permeability of the membranes were compared with the experimental ones. The effect of considering pore size distribution instead of mean pore size to predict the water vapor permeability of the membranes was investigated.

## 1. Introduction

Direct contact membrane distillation (DCMD) is the most used configuration of the membrane distillation (MD) processes [1]. This refers to a thermally driven transport of water through microporous hydrophobic membranes. The membrane is maintained between a hot solution (i.e. feed side) and cold pure water (i.e. permeate side). Due to the hydrophobic nature of the membrane, liquid water cannot penetrate

inside the dry membrane pores unless a transmembrane hydrostatic pressure exceeding the liquid entry pressure of water (*LEPw*), which is characteristic of each membrane, is applied. This condition results in the formation of liquid-vapor interfaces at the entrances of each membrane pore. In this process, the membrane acts only as a physical support for the vapor-liquid interfaces and does not contribute to the separation performance. If a temperature difference is maintained between both sides of the membrane, a transmembrane vapor pressure is created. According to the theory of Non-Equilibrium Thermodynamics, water and volatile molecules evaporate from the hot liquid/vapor interface, cross the pores in vapor phase and condense on the liquid/vapor interface kept at lower temperature.

Other MD configurations, namely, sweeping gas membrane distillation (SGMD), vacuum membrane distillation (VMD) and air gap membrane distillation (AGMD) have been also reported [1–4]. It must be stated that, in the case of solution with non-volatile components such as sodium chloride, only water vapor flows through the membrane. Therefore, the retention degree of solutes is very close to 100%. In this sense, the potential utility of MD for production of high-purity water, concentration of ionic, colloid or other non-volatile aqueous solutions and removal of trace volatile organic compounds (VOCs) from waste water are well recognized [1].

In MD literature, various mathematical models have been proposed to determine the MD flux depending on the considered MD configuration [1–7]. Generally, the analyses were based on the assumption that gas permeates through the porous hydrophobic membrane according to three contributions: Knudsen flow, Poisseuille or viscous flow, molecular diffusion flow and the transition between them.

The physical nature of the mass transport through microporous and hydrophobic membranes was analyzed in DCMD assuming an uniform pore size of the entire membrane [5]. It was concluded that the mass transport takes place via combined Knudsen/molecular diffusion mechanism. Nevertheless, due to pore size distribution of the MD membranes, more than one mechanism of mass transport can occur simultaneously through the entire membrane.

It was reported that the flux of commercial porous membranes, calculated assuming all pores having the same size and the one calculated with a Gaussian (symmetric) function are very similar and the predicted fluxes were lower than the experimental ones [6, 7]. However, in their calculation an adjustment factor (i.e. pore tortuosity) was assumed and mean pore sizes in each mass transfer region (i.e. Knudsen region, continuum region, and transition region) were considered.

In this study, a theoretical approach that considers the gas transport mechanism through each membrane pore individually, without considering any adjustment parameter, is proposed to predict the water vapor permeability of the membrane. Non-interconnected cylindrical pores were assumed. The pore size distribution of each membrane was obtained by means of the wet/dry flow method. The contribution of each mass transport mechanism was investigated. DCMD experiments were carried out using three types of microporous hydrophobic membranes under different temperature conditions. The water vapor permeability of each membrane was

also predicted assuming uniform pore size obtained from the gas permeation test and the wet/dry flow method. The predicted water vapor permeability is compared with the corresponding ones calculated from the experimental DCMD flux using two methods.

## 2. Experimental

### 2.1. Materials

Three microporous hydrophobic flat-sheet membranes: (TF200, Gelman) made of polytetrafluoroethylene supported by a polypropylene net and the (GVHP and HVHP, Millipore) made of polyvinylidene fluoride membranes were used. These membranes are often used in microfiltration process. Their principal characteristics as specified by the manufacturers are the following:

(i)   TF200: nominal pore size = 0.2 μm; void volume = 80%.
(ii)  GVHP: nominal pore size = 0.22 μm; void volume = 75%.
(iii) HVHP: nominal pore size = 0.45 μm; void volume = 75%.

Isopropyl alcohol (GR grade, Merck, Ottawa, Canada) was used as wetting liquid to determine the void volume of the membranes.

### 2.2. Membrane characterization

**2.2.1. Wet/dry flow method**   The bubble point together with the gas permeation tests known as the wet/dry flow method were employed for determining the maximum pore size, the mean pore size and the pore size distribution of the membranes. The procedure and the experimental set-up used were presented in a previous paper [8]. First, the gas permeation velocity, $J_d$, is measured through a dried membrane at different transmembrane pressure differences, $\Delta P$. Then, the membrane is wetted by the isopropyl alcohol (IPA) and again the permeation velocity, $J_w$, is measured for different $\Delta P$ values. In this study, the gas permeation velocity was measured at a temperature of about 25°C maintaining the downstream side at atmospheric pressure. The method suggested by Kesting in [9] was used in our previous study to obtain the pore size distribution [8]. In this paper, an alternative method is proposed in the theoretical section to determine the mean pore size, the geometric standard deviation and the pore size distribution.

**2.2.2. Other membrane characteristics**   The procedures and apparatuses used to obtain the following membrane characteristics were described in detail elsewhere [8].

The *LEPw* is the pressure that must be applied onto pure water before it penetrates into the dried membrane pores. This pressure depends on the pore size and on the hydrophobicity of the membrane. It decreases as the maximum pore size increases and/or the water contact angle decreases.

Membrane void volume, $\varepsilon$, defined as the volume of the pores divided by the total volume of the membrane, was determined by measuring the density of the membrane using isopropyl alcohol (IPA), which penetrates inside the pores of the membrane and pure water, which does not enter the pores.

The average pore size, $\mu_p$, and the effective porosity, $\varepsilon/L_p$, which is defined as the ratio of the porosity and the effective pore length, $L_p$, that takes into account the tortuosity of the membrane pores, have been determined using the gas permeation method. In this study, air was used as standard gas.

The membrane thickness, $\delta$, was measured with a micrometer Millitron (Mahr Feinprüf, Göttingen, Germany, type 1202 IC), with a precision of $\pm 0.1$ μm, on more than ten spots for each membrane sample and the average values are given in this study together with the standard deviation. Due to the fact that TF200 membrane is supported by a backing propylene net, the membrane layer was pilled off from the support and its thickness was measured.

**2.2.3. Direct contact membrane distillation**  DCMD experiments were carried out by using the experimental system described elsewhere [5]. The experiments were conducted with pure water as feed. The central part of the system is a stainless steel cell composed of two cylindrical chambers. One of the chambers is connected to a heating system through its jacket to control the temperature of the liquid feed. The other chamber is connected to a cooling system to control the temperature of the permeate. The membrane was placed between the two chambers. The effective membrane area is $2.75 \, 10^{-3} \, m^2$. The DCMD flux was calculated in every case by measuring the condensate collected in the permeate chamber for a predetermined period.

# 3. Theoretical

## 3.1. Mean pore size and pore size distribution: Analysis of data obtained from wet/dry flow method

The wet/dry flow method was used to determine the mean pore size, the geometric standard deviation and the pore size distribution. It was observed, for each wetted membrane by isopropyl alcohol (IPA), that the pores remain filled with IPA at low transmembrane pressure, $\Delta P$, and the gas permeation velocity through the membrane, $J_w$, is practically zero [8]. At a certain value of $\Delta P$ corresponding to the bubble point of the membrane, the largest pores will be opened and the gas permeation velocity starts to increase. Smaller membrane pores are opened as $\Delta P$ increases according to the Laplace equation. Finally, at the pressure corresponding to the minimum pore size, all the pores become empty. The ratio $J_w/J_d$ is unity when $\Delta P$ is higher than this pressure and the flow curve returned to that obtained with a membrane dry sample. The two runs (dry and wet curves) permit the determination of the mean pore size, geometric standard deviation and pore size distribution using the following procedure:

For all pores with sizes below $d_p(j)$, i.e. pore in class $j^{\text{th}}$ $(j = 1\ldots n)$, the cumulative flow can be written as:

$$g_a(j) = 1 - g_a'(j) = 1 - \frac{J_w(j)}{J_d(j)} \tag{1}$$

The differential flow through pores in class $j^{\text{th}}$ with a pore diameter $d_p(j)$ is:

$$g_d(j) = \frac{g_a'(j+1) - g_a'(j-1)}{2} \tag{2}$$

Taking into account that the flow is proportional to the pore area, the number of pores with size $d_p(j)$ is:

$$n_d(j) = K\frac{g_d(j)}{d_p(j)^2} \tag{3}$$

where $K$ is a normalization factor that can be evaluated as:

$$K = \frac{g_a(n)}{\sum_{j=1}^{n} g_d(j)/d_p(j)^2} \tag{4}$$

Finally, the cumulative distribution of number of pores is:

$$n_a(j) = \sum_{k=1}^{j} n_d(k) \tag{5}$$

As stated in a previous paper based on atomic force microscopy analysis [10], the pore size distribution can be expressed by the probability density function (i.e. log-normal distribution) described by the following equation:

$$\frac{df(d_p)}{d(d_p)} = \frac{1}{d_p \ln \sigma_p (2\pi)^{1/2}} \exp\left(-\frac{(\ln d_p - \ln \mu_p)^2}{2(\ln \sigma_p)^2}\right) \tag{6}$$

where $d_p$ is the pore size, $\sigma_p$ is the geometric standard deviation and $\mu_p$ is the mean pore size of the membrane.

In this study, the function $f(d_p)$ was used to fit the obtained cumulative distribution of relative number of pores, $n_a(j)$. The mean pore size, $\mu_p$, together with the geometric standard deviation, $\sigma_p$, were then determined for each membrane.

In addition, the surface porosity, $\varepsilon_s$, defined as the ratio between the area of the pores to the total membrane surface area, can be calculated from Eq. (7).

$$\varepsilon_s = \frac{N\pi}{4} \sum_{j=1}^{n} f_j d_j^2 \tag{7}$$

where $N$ is the number of pores per unit area, known as pore density and $f_j$ is the fraction of the number of pores with size $d_j$.

It must be stated that the surface porosity, $\varepsilon_s$, is different to the void volume, $\varepsilon$.

$$\varepsilon = \varepsilon_s \tau \tag{8}$$

where $\tau$ is the pore tortuosity.

Finally, if the effective membrane porosity, which takes into account the tortuosity of the membrane pores (i.e. $\varepsilon/L_p = \varepsilon/\tau\delta$) is known, the number of pores per unit area can be calculated from the following equation:

$$N = \frac{\delta(\varepsilon/L_p)}{\sum_{j=1}^{n} f_j \pi r_j^2} = \frac{\varepsilon/\tau}{\sum_{j=1}^{n} f_j \pi r_j^2}. \tag{9}$$

### 3.2. Prediction of membrane water vapor permeability from pore size distribution

The transport of gas through porous media has been studied with theoretical models based on the kinetic theory of gases and different transport mechanisms have been proposed [1–5]. Non-interconnected cylindrical pores were assumed.

Due to the fact that in DCMD configuration both feed and permeate aqueous solutions are brought into contact with the membrane under atmospheric pressure, the total pressure is constant at $\approx 1$ atm resulting in negligible viscous flow [1, 5].

In DCMD, mass transport across the membrane with different pore sizes occurs in three regions depending on the pore size and the mean free path, $\lambda_w$, of the transferring species [1, 11]: Knudsen region, continuum region (or ordinary diffusion region) and transition region (or combined Knudsen/ordinary diffusion region).

It must be pointed out that the Knudsen number, $Kn$, defined as the ratio of the mean free path of the gas to the pore size, provides a guideline in determining which mechanism is operative in a given pore under given experimental conditions. The mean free path can be calculated for water vapor using the following expression [12]:

$$\lambda_w = \frac{k_B T}{\sqrt{2}\pi \bar{p} \sigma_w^2} \tag{10}$$

where $\sigma_w$ is the collision diameter (for water vapor is 2.641 Å), $k_B$ is the Boltzmann constant, $\bar{p}$ the mean pressure within the membrane pores (the total pressure is 101.325 kPa for DCMD) and $T$ the absolute temperature.

In the Knudsen region, the mean free path of the water molecules is large in relation with the membrane pore size (i.e. $Kn > 1$ or $d_p < \lambda_w$) and the molecule-pore wall collisions are dominant over the molecule-molecule collisions. In this case the water vapor permeability through a single cylindrical pore can be expressed as follows [12]:

$$B_w^K = \frac{2\pi}{3} \frac{1}{RT} \left(\frac{8RT}{\pi M_w}\right)^{1/2} \frac{r_k^3}{\tau\delta} \tag{11}$$

where $r_k$ is the pore radius in the Knudsen region, $M_w$ is the molecular weight of water, $R$ is the gas constant and $\delta$ is the membrane thickness.

If $Kn < 0.01$ (i.e. $d_p > 100\lambda_w$), molecular diffusion is used to describe the mass transport in continuum region caused by the virtually stagnant air trapped within each membrane pore due to the low solubility of air in water. In this case the following relationship can be used for the water vapor permeability of a pore having an area of $\pi r_D^2$ in the ordinary diffusion region [1].

$$B_w^D = \frac{\pi}{RT} \frac{PD}{p_a} \frac{r_D^2}{\tau\delta} \tag{12}$$

where $D$ is the water diffusion coefficient, $P$ is the total pressure inside the pore, assumed constant, and equal to the sum of the partial pressures of air and water vapor, and $p_a$ is the air pressure in the membrane pore. In this study, the value of $PD$ (Pa m$^2$/s) for water-air was calculated from Eq. (13) [7].

$$PD = 1.895 \ 10^{-5} T^{2.072} \tag{13}$$

In transition region, $0.01 < Kn < 1$ (i.e. $\lambda < d_p < 100\lambda$), the mass transport takes place via a combined Knudsen/ordinary diffusion mechanism and the following model is used to determine the water vapor permeability [1].

$$B_w^C = \frac{\pi}{RT} \frac{1}{\tau\delta} \left[ \left(\frac{2}{3}\left(\frac{8RT}{\pi M_w}\right)^{1/2} r_t^3\right)^{-1} + \left(\frac{PD}{p_a} r_t^2\right)^{-1} \right]^{-1} \tag{14}$$

where $r_t$ is the pore radius in transition region.

For a membrane having a distribution of pore size, all the above cited mechanisms can occur simultaneously, but to different extents, depending on the operating conditions. Therefore, the total DCMD water vapor permeability of the membrane can be estimated by considering each pore by applying the relevant equation through it and then summing the water vapor permeabilities over the entire system of pores. Non-interconnected cylindrical pores are assumed. Consequently, the total water vapor permeability of the membrane in DCMD configuration, $B_w^m$, can be written as:

$$B_w^m = \frac{N}{\delta} \left[ \sum_{j=1}^{m \ (r=0.5\lambda_w)} G_w^K f_j r_j^3 + \sum_{j=m \ (r=0.5\lambda_w)}^{p \ (r=50\lambda_w)} \left(\frac{1}{G_w^K r_j} + \frac{1}{G_w^D}\right)^{-1} f_j r_j^2 + \sum_{j=p \ (r=50\lambda_w)}^{n \ (r=r_{max})} G_w^D f_j r_j^2 \right] \tag{15}$$

where

$$G_w^K = \left(\frac{32\pi}{9M_wRT}\right)^{1/2} \tag{16}$$

$$G_w^D = \frac{\pi}{RT}\frac{PD}{p_a} \tag{17}$$

and $f_j$ is the fraction of pores with pore radius $r_j$, $N$ is the total number of pores per unit area, $m$ is the last class of pores in Knudsen region and $p$ is the last class of pores in the transition region.

It is to be noted that in Eq. (15) the upper limit of each summation is altered depending on the maximum pore radius $(r_{max})$. The following three cases are possible: (1) if $(r_{max} < 0.5\lambda_w)$, only Knudsen mechanism prevails; (2) if $(0.5\lambda_w < r_{max} < 50\lambda_w)$ both Knudsen and transition mechanisms are applicable; and (3) if $(r_{max} > 50\lambda_w)$ all mechanisms are operative simultaneously.

### 3.3. Prediction of membrane water vapor permeability from mean pore size

Eq. (15) can be simplified when an uniform pore radius $\langle r \rangle$ is assumed. Namely, when $\langle r \rangle < 0.5\lambda_w$, Knudsen model is applied and Eq. (15) can be written as [1]:

$$B_w^m = \frac{2}{3RT}\frac{\varepsilon\langle r \rangle}{\tau\delta}\left(\frac{8RT}{\pi M_w}\right)^{1/2} \tag{18}$$

while, when $0.5\lambda_w < \langle r \rangle < 50\lambda_w$, the transition flow will dominate and Eq. (15) is written as [1]:

$$B_w^m = \frac{1}{RT\delta}\left[\frac{3\tau}{2\varepsilon\langle r \rangle}\left(\frac{\pi M_w}{8RT}\right)^{1/2} + \frac{P_a\tau}{\varepsilon PD}\right]^{-1} \tag{19}$$

### 3.4. Calculation of the water vapor permeability from DCMD experiments

**3.4.1. Method 1**   The molar flux of water vapor, $F_w$, is linearly related to its partial pressure difference across the membrane pores as stated in previous papers [1, 5].

$$F_w = B_w^m(p_{m,f} - p_{m,p}) \tag{20}$$

where $p_{m,f}$ and $p_{m,p}$ are the water partial pressures of the feed and permeate at the membrane surface, respectively.

The water vapor pressures within the membrane are not directly measurable, then it is convenient to express Eq. (20) in terms of temperatures. For low values of the transmembrane bulk temperature difference $(T_{b,f} - T_{b,p} \leq 10 \text{ K})$, the following expression may be used as indicated in [13].

$$F_w = B_w^m \left(\frac{dp}{dT}\right)_{Tm} (T_{m,f} - T_{m,p}) \tag{21}$$

where $T_m$ is the mean temperature and $(dp/dT)$ can be evaluated from the Clausius-Clapeyron equation, using Antoine equation to calculate the vapor pressure [1, 13].

$$\left(\frac{dp}{dT}\right)_{Tm} = \left[\frac{\Delta H_v}{RT^2} \exp\left(23.238 - \frac{3841}{T - 45}\right)\right]_{Tm} \tag{22}$$

where $\Delta H_v$ is the water heat of vaporization.

Additionally, it is well known that in DCMD processes, simultaneous heat and mass transfers through the membrane occur and the temperatures at the vapor-liquid interfaces differ from the temperatures at the bulk phases, due to the temperature polarization effect. The heat transfer within the membrane is due to the latent heat accompanying vapour flux and the heat transferred by conduction across the membrane material and across the gas-filled pores. Thus the overall process rate appears to be controlled by the heat and mass transfer through both the membrane and liquid phases and the following equations are applied [1, 5].

$$h_f(T_{b,f} - T_{m,f}) = \frac{k_m}{\delta}(T_{m,f} - T_{m,p}) + F_w\Delta H_v = h_p(T_{m,p} - T_{b,p}) \tag{23}$$

where $h_f$ and $h_p$ are the heat transfer coefficients in the feed and permeate liquid, respectively; and $k_m$ is the thermal conductivity of the membrane, which can be calculated as [1]:

$$k_m = \varepsilon k_g + (1 - \varepsilon)k_s \tag{24}$$

with $k_g$ and $k_s$ are the thermal conductivities of the gas phase and of the solid phase, respectively.

From Eqs. (21–23), the following expression may be reached [13].

$$\frac{T_{b,f} - T_{b,p}}{F_w\Delta H_v} = \frac{1 + \frac{k_m}{\delta h}}{B_w^m\Delta H_v \frac{dp}{dT}} + \frac{1}{h} \tag{25}$$

where, $h$ is the heat transfer coefficient, defined as:

$$h = \left(\frac{1}{h_f} + \frac{1}{h_p}\right)^{-1} \tag{26}$$

Eq. (25) may be used for the analysis of experimental results for which the bulk feed and permeate temperatures together with the DCMD flux are known. A fit to a linear function of $(T_{bf} - T_{bp})/(F_w\Delta H_v)$ versus the corresponding values of $[\Delta H_v(dp/dT)]^{-1}$

should yield an intercept of $1/h$ and a slope of $(1/B_w^m \Delta H_v)(1 + k_m/\delta h)$, from which $B_w^m$ may be obtained.

### 3.4.2. Method 2: Semi-empirical model

The membrane temperature may be different from the one calculated for the bulk phases due to the fact that the heat transfer coefficients at each side of the membrane are expected to be different as the temperature and therefore the density, viscosity, thermal conductivity, heat capacity, etc. are different. As a consequence the temperature polarization in each phase adjoining the membrane, feed and permeate, must be different. On the other hand, the membrane permeability depends on temperature as can be expected from Eqs. (11), (12) and (14). However, Eq. (25) permits to get a constant value of the membrane permeability as stated earlier, according to Eq. (25). A semi-empirical method can be used to determine the $B_w^m$ values as function of temperature without using the linearization of the exponential dependence of the vapor pressure with temperature, applied in Eq. (21), valid only for small temperature differences between feed and permeate and for water and dilute aqueous solutions.

Eq. (23) permits to write the temperatures $T_{m,f}$ and $T_{m,p}$ as:

$$T_{m,f} = \frac{\dfrac{k_m}{\delta}\left(T_{b,p} + \dfrac{h_f}{h_p}T_{b,f}\right) + h_f T_{b,f} - F_w \Delta H_v}{\dfrac{k_m}{\delta} + h_f\left(1 + \dfrac{k_m}{\delta h_p}\right)} \tag{27}$$

$$T_{m,p} = \frac{\dfrac{k_m}{\delta}\left(T_{b,f} + \dfrac{h_p}{h_f}T_{b,p}\right) + h_p T_{b,p} + F_w \Delta H_v}{\dfrac{k_m}{\delta} + h_p\left(1 + \dfrac{k_m}{\delta h_f}\right)} \tag{28}$$

In the above equations the heat transfer coefficients for turbulent liquid flow, $h_f$ and $h_p$, can be determined by means of the following semi-empirical correlation [1].

$$Nu = 0.027 Re^{4/5} Pr^m \left(\frac{\mu_b}{\mu_m}\right)^{0.14} \tag{29}$$

where $Nu, Re$ and $Pr$ are Nusselt, Reynolds and Prandtl numbers, respectively; the superscript $m$ is 0.4 for heating and 0.3 for cooling; $\mu_b$ and $\mu_m$ are the water dynamic viscosity at the bulk and at the membrane surface, respectively.

In order to determine $B_w^m$, the following steps were carried out: Initially, a mean temperature is used to calculate the $Re, Pr$ and $Nu$ numbers. Subsequently, the membrane surface temperatures ($T_{m,f}$ and $T_{m,p}$) are calculated by applying Eqs. (27) and (28). The mean temperature $(T_{m,f} + T_{m,p})/2$ is evaluated and the $Re, Pr$ and $Nu$ numbers are calculated again. This procedure is repeated until the difference between two successive mean temperatures is less than $10^{-7}$%. Finally, the vapor pressure of the feed and permeate at the membrane surface is determined from the last values of $T_{m,f}$ and $T_{m,p}$ and the membrane permeability is calculated using Eq. (20).

## 4. Results and discussion

### 4.1. Results on morphological characterization of MD membranes

Table 1 lists the obtained characteristics of the studied membranes. It can be observed that the membrane TF200 exhibits higher $LEPw$ values than the GVHP one. This may be attributed to the lower maximum pore size and to the higher hydrophobicity of the polytetrafluoroethylene polymer. For the membranes GVHP and HVHP prepared with the same polymer (i.e. polyvinylidene fluoride), the $LEPw$ of the HVHP membrane is lower than that of the GVHP one. This is due to the higher pore size of the membrane HVHP.

The void volume of the membranes GVHP and HVHP are specified as 75% by the manufacturer, while that of TF200 is 80%. However, the measured void volume of these membranes (Table 1) are lower than these values. This may be attributed to the different techniques used. Moreover, the membranes GVHP and HVHP are thicker than the membrane TF200. This may induce lower effective membrane porosity for these membranes, as found from the gas permeation test. In fact, the effective porosity is about 2.8 and 2.7 times higher for the membrane TF200 than for the membranes GVHP and HVHP, respectively.

It must be stated that the mean pore size of the membrane TF200, determined from the gas permeation test, is almost the same as the value given by the manufacturer, while those obtained for the membranes GVHP and HVHP were higher.

The average pore size and the pore size distribution of the membranes were also determined by the wet/dry flow method as stated earlier. In Figure 1, the cumulative pore size distribution data obtained from Eqs. (1–5) are shown together with the fitting curves to the log-normal distribution function. Reasonably high correlation coefficients were obtained for all membranes ($r^2 > 0.996$). The mean pore size and the geometric standard deviation were determined from the fitting curves. The results are given in Table 2. From these data the probability density function curves were generated for both membranes and presented in Figure 2.

**Table 1** Membrane characteristics: membrane thickness, $\delta$; liquid entry pressure of water, $LEPw$; void volume, $\varepsilon$; mean pore size, $\mu_p$; effective porosity, $\varepsilon/L_p$.

| Membrane | $\delta$ (µm) | $LEPw$ (bar) | $\varepsilon$ (%) | Gas permeation test[d] | |
|---|---|---|---|---|---|
| | | | | $\mu_p$ (nm) | $\varepsilon/L_p$ (m$^{-1}$) |
| TF200[a] | 55 ± 6 | 2.76 ± 0.09 | 69 ± 5 | 198.96 | 7878.1 |
| GVHP[b] | 118 ± 4 | 2.04 ± 0.03 | 70 ± 3 | 283.15 | 2781.9 |
| HVHP[b] | 116 ± 3 | 1.05 ± 0.04 | 71 ± 2 | 463.86 | 2904.7 |

a. Membrane supplied by Gelman. Measured total thickness: 165 ± 8 µm.
b. Membranes supplied by Millipore.
d. $\mu_p, \varepsilon/L_p$ were determined from the gas permeation test.
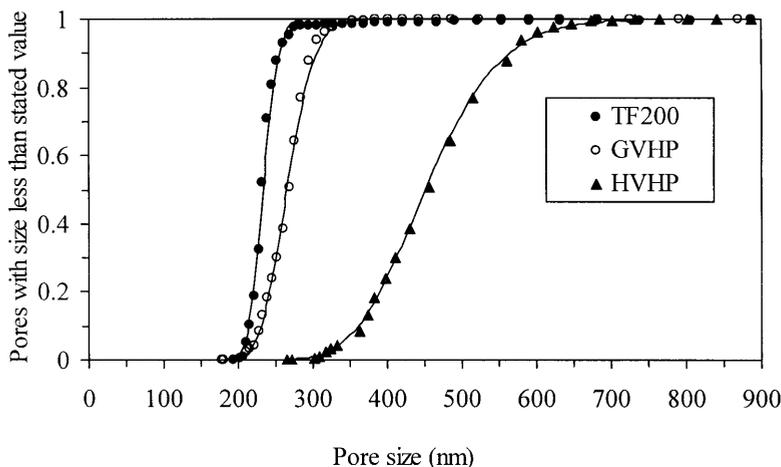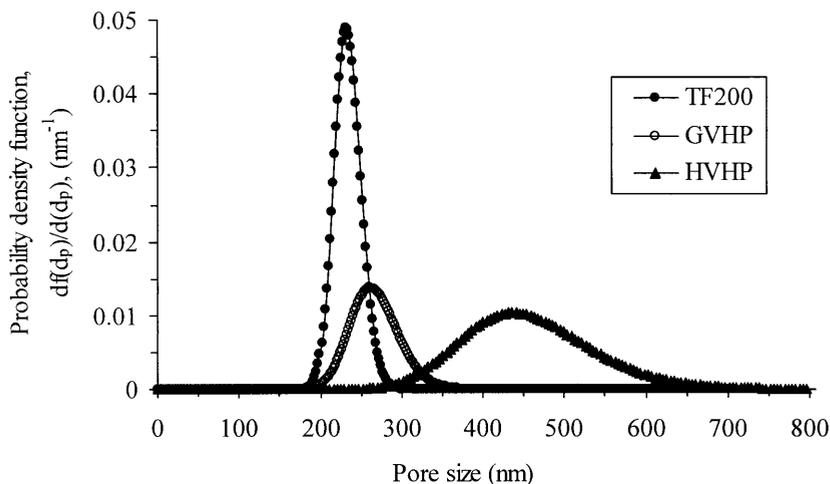
**Figure 1** Cumulative pore size distribution of the membranes TF200, GVHP and HVHP obtained from the wet/dry flow method.

**Table 2** Results of the wet/dry flow method. Mean pore size, $\mu_p$; geometric standard deviation, $\sigma_p$; pore density, $\rho_s$; surface porosity, $\varepsilon_s$, pore tortuosity, $\tau$.

| Membrane | $\mu_p$ (nm) | $\sigma_p$ | $N$ ($\mu m^{-2}$) | $\varepsilon_s$ (%) | $\tau$ |
|----------|----------|--------|-----------------|-----------|------|
| TF200 | 233.38 | 1.07 | 9.87 | 43.18 | 1.59 |
| GVHP | 265.53 | 1.12 | 5.73 | 32.74 | 2.14 |
| HVHP | 451.23 | 1.19 | 1.96 | 33.64 | 2.12 |

From Figures 1 and 2 it can be observed that the pore size distribution curve of the membrane TF200 is higher and narrower around the mean pore size and is shifted to the left in comparison to the pore size distributions of the membranes GVHP and HVHP. The mean pore sizes of the membranes, determined from the wet/dry flow method, follow the same sequence as those determined from the gas permeation test. However, the mean pore sizes determined from the wet/dry flow method are 6.2% and 2.7% lower than those obtained from the gas permeation test for the membranes GVHP and HVHP, respectively. For the TF200 membrane the mean pore size determined from the wet/dry flow method is 17.3% larger than that determined from the gas permeation test. Other authors [7], by using the field emission scanning electron microscopy (FESEM), reported mean pore sizes of 251 nm for GVHP membrane and 414 nm for HVHP membrane, which are slightly lower than the ones obtained in this study from the gas permeation test and the wet/dry flow method. This may be attributed to pore contraction during metal-coating of the membrane sample, which is required to produce the FESEM images.

In addition, the obtained values of the geometrical standard deviation, $\sigma_p$, of all membranes were close to unity although the Millipore membranes and the Gelman one were prepared with different polymers and different techniques.

**Figure 2** Probability density curves of the membranes TF200, GVHP and HVHP membranes.

Pore density, $N$, and surface porosity, $\varepsilon_s$, were calculated using the pore size distributions (Figure 2) and Eqs. (9) and (7), respectively. The results are also summarized in Table 2. In comparison to the membrane TF200, it can be seen that the pore density and surface porosity of the Millipore membranes are lower; while the void volume given in Table 1 are higher. This may be attributed to the larger thickness and to the higher pore tortuosity of the Millipore membranes.

The tortuosity factor was calculated from the void volume, $\varepsilon$, and the effective porosity, $\varepsilon/L_p$, determined by the gas permeation test. $L_p$ is the effective pore length that takes into consideration the tortuosity effect (i.e. $L_p = \tau\delta$). The so obtained values are given in Table 2. The calculated pore tortuosity of the membranes GVHP and HVHP are higher than that of the membrane TF200. This may be attributed to the higher membrane thickness of the Millipore membranes and also to the different polymers (i.e. PTFE, PVDF) and membrane preparation techniques used. In MD studies, a value of 2 is frequently assumed for tortuosity factor [1, 7, 13].

## 4.2. Water vapor permeability of the membranes

The dependence of the involved operating parameters such as feed and permeate temperatures and circulation velocities on the mass transfer in DCMD applications has been investigated previously [1, 14]. In this study, the water vapor permeability of the membranes was obtained using pure water as feed. The conditions of the experiments were 500 rpm stirring rate in both chambers, mean temperatures varying from 20°C to 55°C, with steps of 5°C and bulk temperature difference of 10°C. In Figure 3, the measured flux is plotted versus the mean temperature. The increase of the flux with the mean temperature may be explained from the exponential increase of the vapor pressure with temperature, as stated by Antoine's equation. The data in
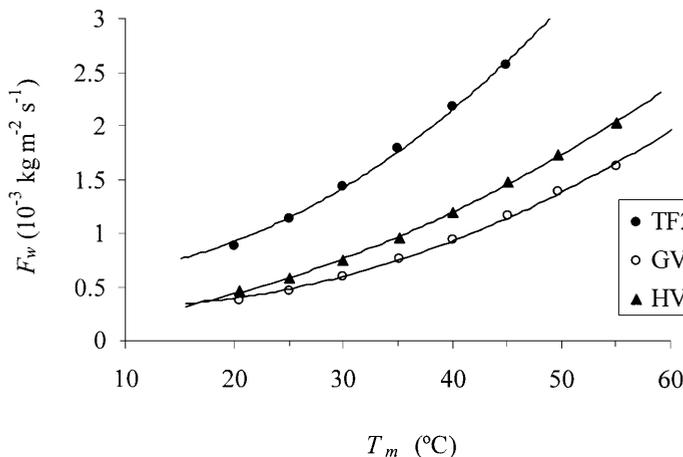
**Figure 3**  DCMD flux vs. mean temperature. Stirring rate, 500 rpm; bulk temperature, 10°C.

Figure 3 were fitted according to the following expression by the using the non-linear $\chi^2$ minimization method as reported in [14]:

$$F_w \propto \frac{1}{T_m} \exp\left(-\frac{\Delta H_v}{RT_m}\right) \tag{30}$$

The obtained correlation coefficients are higher than 0.995. It can be seen that the DCMD flux of the TF200 membrane was higher than that obtained by using the GVHP and HVHP membranes. This result may be due to the higher tortuosity factor and higher thickness of the later membranes. Moreover, the flux of the membrane HVHP is higher than that of the membrane GVHP. This is due to the larger pore size of the membrane HVHP.

The heat transfer coefficient, $h$, and the water vapor permeability, $B_w^m$, have been obtained from the experimental data presented in Figure 3 according to the method 1 (Eq. 25). It is worth mentioning that $dp/dT$ was evaluated for the average temperature determined from the bulk feed and permeate temperatures. The results of both membranes are shown in Figure 4. Straight lines, with reasonably high correlation coefficients ($r^2 > 0.999$), are obtained. The $h$ values determined from the intercept of the lines are $(31 \pm 2) \times 10^2$ W m$^{-2}$ K$^{-1}$ for TF200 membrane, $(35 \pm 3) \times 10^2$ W m$^{-2}$ K$^{-1}$ for GVHP membrane and $(46 \pm 5) \times 10^2$ W m$^{-2}$ K$^{-1}$ for HVHP membrane.

In order to evaluate the $B_w^m$ coefficients from the slope of the lines in Figure 4, the thermal conductivity of the porous membranes $k_m$ was estimated from the following values: $k_g = 0.027$ W m$^{-1}$ K$^{-1}$, $k_s = 0.22$ W m$^{-1}$ K$^{-1}$ for TF200 and $k_s = 0.126$ W m$^{-1}$ K$^{-1}$ for GVHP membrane [15, 16]. Under the present experimental conditions, the obtained values of the thermal conductivity, $k_m$, using Eq. (24) lies between 0.054 W m$^{-1}$ K$^{-1}$ and 0.057 W m$^{-1}$ K$^{-1}$ for GVHP and HVHP membranes, while for TF200 membrane $k_m$ values are between 0.086 W m$^{-1}$ K$^{-1}$ and
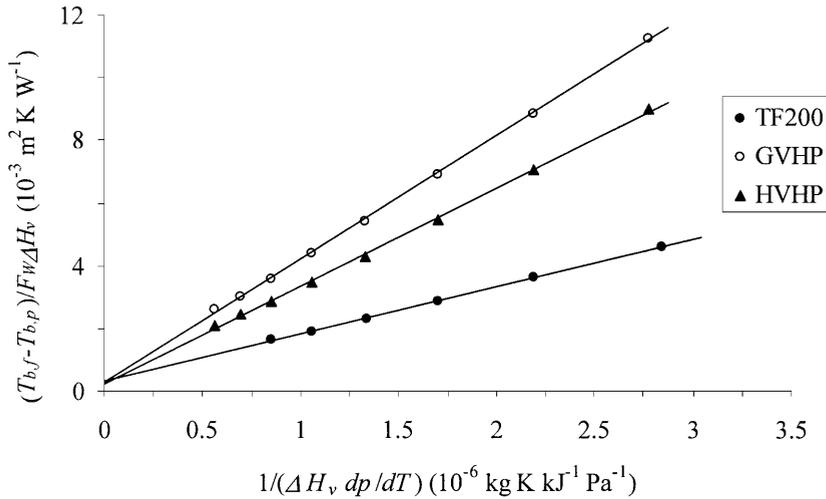
**Figure 4** Plots of Eq. (25) of the experimental data given in Figure 3 for TF200, GVHP and HVHP membranes.

0.088 W m$^{-1}$ K$^{-1}$. These values are higher than those determined experimentally in [4] for the same membranes (0.041 W m$^{-1}$ K$^{-1}$ for GVHP and HVHP membranes and 0.043 W m$^{-1}$ K$^{-1}$ for the membrane TF200). By using the calculated $k_m$ values from Eq. (24) or the experimental ones adopted from [4], the calculated membrane permeability variation is less than $4 \times 10^{-6}$ % for the membranes GVHP and HVHP, and less than $4 \times 10^{-5}$ % for the membrane TF200. The obtained $B_w^m$ values are $(667 \pm 5) \times 10^{-9}$ kg m$^{-2}$ s$^{-1}$ Pa$^{-1}$ for the membrane TF200, $(255 \pm 2) \times 10^{-9}$ kg m$^{-2}$ s$^{-1}$ Pa$^{-1}$ for the membrane GVHP and $(320 \pm 4) \times 10^{-9}$ kg m$^{-2}$ s$^{-1}$ Pa$^{-1}$ for the membrane HVHP.

The permeability of each membrane was also calculated using the semi-empirical model (Method 2). The results are summarized in Table 3, as function of the mean temperature, for each membrane. For all membranes, it can be seen that $B_w^m$ increases with temperature and are higher than the ones obtained from Eq. (25) (Method 1).

Under the experimental conditions used in this study, the calculated mean free path of water vapor, $\lambda_w$, increases from 128.9 nm to 146.5 nm as the mean temperature increases from 20°C to 60°C. From the data presented in Figures 1 and 2, it was found that the maximum pore size of both membranes is lower than $100\lambda_w$ and only Knudsen and transition regions are taken into account. Therefore, Eq. (15) can be modified by neglecting the third term corresponding to the ordinary diffusion region. Hence, the membranes having pores with size (i.e. diameter) below $\lambda_w$ lend themselves to the Knudsen region and all pores having sizes between $\lambda_w$ and $100\lambda_w$ are considered in transition region. The proportions of Knudsen and transition regions can be evaluated by the cumulative pore size distribution presented in Figure 1. It was found that the mass transport has a major contribution in the transition region for all membranes (i.e. more than 98.7%). This means that the majority of membrane area belongs to the combined Knudsen/ordinary diffusion region.

**Table 3** Water vapor permeability of the membranes, $B_w^m$, in ($10^{-9}$ kg m$^{-2}$ s$^{-1}$ Pa$^{-1}$).

| Membrane | Model | Temperature (°C) | | | | | | | | |
|---|---|---|---|---|---|---|---|---|---|---|
| | | 20 | 25 | 30 | 35 | 40 | 45 | 50 | 55 | 60 |
| TF200 | I | 900.5 | 903.4 | 917.3 | 931.8 | 951.2 | 969.8 | – | – | – |
| | II | 939.8 | 953.2 | 968.1 | 984.8 | 1003.9 | 1026.0 | 1052.1 | 1083.3 | 1121.1 |
| | III | 934.8 | 948.1 | 962.7 | 979.2 | 998.0 | 1019.8 | 1045.5 | 1076.2 | 1113.4 |
| | IV | 881.2 | 892.6 | 905.1 | 919.2 | 935.2 | 953.8 | 975.8 | 1002.0 | 1033.6 |
| GVHP | I | 337.4 | 339.8 | 343.1 | 349.7 | 353.8 | 362.3 | 370.5 | 382.0 | – |
| | II | 347.6 | 353.0 | 358.9 | 365.6 | 373.2 | 382.0 | 392.5 | 405.0 | 420.2 |
| | III | 344.8 | 350.0 | 355.8 | 362.3 | 369.8 | 378.4 | 388.6 | 400.8 | 415.6 |
| | IV | 351.8 | 357.4 | 363.5 | 370.4 | 378.2 | 387.3 | 398.1 | 411.0 | 426.7 |
| HVHP | I | 426.7 | 434.7 | 441.3 | 452.1 | 465.6 | 480.5 | 493.6 | 517.1 | – |
| | II | 420.2 | 428.3 | 437.3 | 447.4 | 459.0 | 472.6 | 488.7 | 508.2 | 532.2 |
| | III | 415.1 | 423.0 | 431.7 | 441.5 | 452.8 | 465.9 | 481.4 | 500.2 | 523.3 |
| | IV | 417.6 | 425.6 | 434.5 | 444.4 | 455.8 | 469.1 | 485.0 | 504.1 | 527.6 |

I: ($B_w^m$ values calculated from the semi-empirical model, Method 2);
II: ($B_w^m$ values predicted from Eq. (15) by considering the pore size distribution);
III: ($B_w^m$ values predicted from Eq. (19) by considering the mean pore size obtained from wet/dry flow method);
IV: ($B_w^m$ values predicted from Eq. (19) by considering the mean pore size determined from gas permeation test).

The water vapor permeability of both membranes were calculated for each temperature, from 20 to 60°C, using the pore size distribution (Figure 2) and Eqs. (15–17). The considered total pressure within the membrane pores is atmospheric pressure and the temperatures were similar to those stated previously to generate Figures 3 and 4. The predicted $B_w^m$ values of all membranes are given in Table 3 as function of the mean temperature (rows II in Table 3). For the tested membranes, it can be seen that the predicted water vapor permeability increases with the mean temperature and is higher for the membrane TF200. However, from Knudsen flow model (Eq. 11), the mass transport is inversely proportional to the temperature. This indicates that for all membranes the predominant transport mechanism is the molecular diffusion. In fact, the highest contribution to the total flux of Knudsen flux is $1.0 \times 10^{-6}$% for GVHP membrane, $3.0 \times 10^{-10}$% for HVHP membrane and $5.2 \times 10^{-10}$% for TF200 membrane. As stated earlier, from the pore size distribution, Knudsen contribution is very low while practically 99% of pores are in the transition region. As an example, Figure 5 shows the variation of the water vapor permeability versus pore size of the membranes GVHP and TF200, when the mean temperature is 40°C. At this temperature, the mean free path of water vapor is about 137.7 nm. A visual inspection of Figure 5 suggests that the ordinary flow model is predominant for mass transport in DCMD configuration as all the pores having pore size lower than 137.7 nm have $B_w^m$ values near zero for both membranes.

It must be pointed out that for the membranes GVHP and TF200, the predicted water vapor permeability considering pore size distributions, Eq. (15), is slightly higher than the calculated ones from the semi-empirical model (Method 2). However, for the membrane HVHP the calculated permeability using method 2 is slightly higher than that obtained considering pore size distribution and Eq. (15).
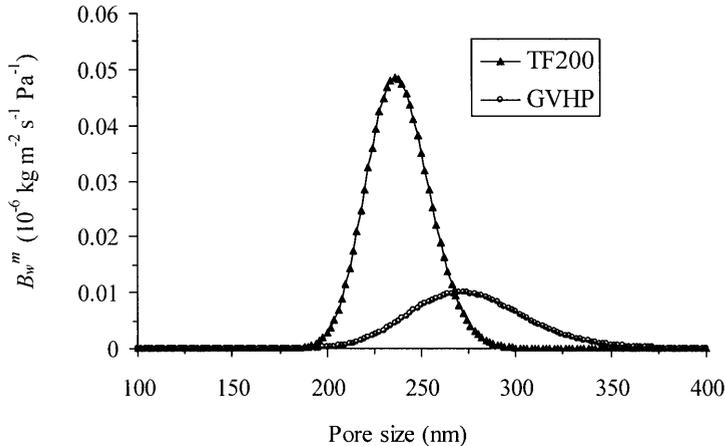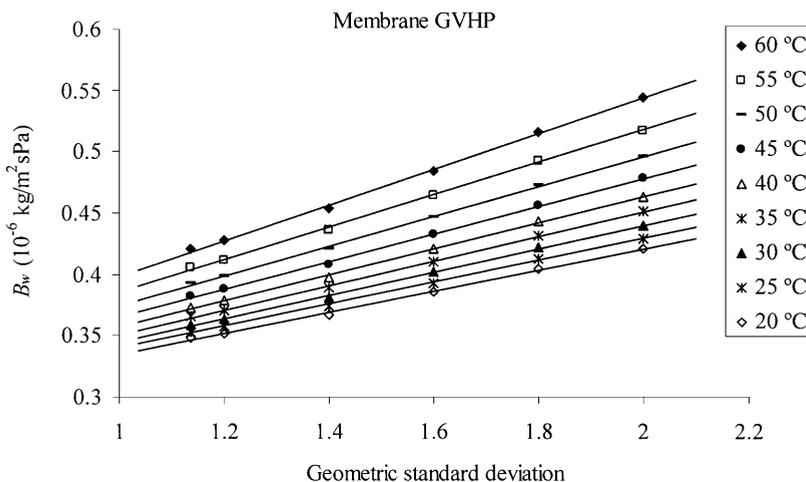
**Figure 5**   Calculated water vapor permeability, $B_w^m$, vs. pore size of the membranes GVHP and TF200 at mean temperature, $T_m$, 40°C.

In addition, the effects of the pore size distribution on the water vapor permeability was examined by comparing the water vapor permeability calculated from Eq. (15), which takes into account the pore size distributions with those obtained from Eqs. (18) and (19), in which an uniform pore size (i.e. mean pore size) is assumed. In the latter calculation, two different sources of the mean pore sizes; i.e. one obtained from gas permeation experiments (Table 1) and the other obtained by the wet/dry flow method (Table 2), were used.

In the studied range of temperatures, the mean pore sizes are between $\lambda_w$ and $100\lambda_w$. Therefore, the mean pore sizes belonged to the transition region and Eq. (19) was used. The results are also shown in Table 3 (rows III and IV).

Comparing the water vapor permeability calculated with the pore size distribution and with the mean pore sizes (given in Table 2), both obtained from the wet/dry flow method, those calculated by including the effect of pore size distribution were slightly higher than those predicted from the mean pore size. This may be attributed to the low values of the geometric standard deviations, which were found to be near unity for the three membranes. This is a common characteristic of commercial membranes. If other porous membranes with higher geometric standard deviations are used, larger discrepancy may be detected between the predicted values including pore size distribution and those predicted assuming uniform mean pore size for all membrane area. This statement is evident in Figure 6, which shows the effect of the geometric standard deviation on the water vapor permeability of the membrane GVHP for each mean temperature. Similar curves can be plotted for the other two membranes. For the membrane TF200, the enhancement of the water vapor permeability is 24.4% at 20°C and 33.9% at 60°C when the geometric standard deviation increases from 1.07 to 2. For the membrane HVHP, the increase is 12.0% at 20°C and 17.3% at 60°C when the geometric standard deviation increases from 1.19 to 2.

**Figure 6**   Predicted water vapor permeability of the membrane GVHP, $B_w^m$, vs. geometric standard deviation at different temperatures.

Table 3 also shows the predicted water vapor permeability using the mean pore size and the effective porosity determined from the gas permeation test (rows IV in Table 3). For GVHP membrane the obtained $B_w^m$ values were slightly higher than those obtained using the pore size distribution. In contrast, for TF200 and HVHP membranes the predicted $B_w^m$ values for the mean pore size determined based on the gas permeation test were lower than those predicted by considering pore size distribution.

From the data given in Table 3, the discrepancy between the predicted water vapor permeabilities from the different methods is 7.8% for the membrane TF200, 7.6% for the membrane GVHP and 3.3% for the membrane HVHP, in the worst case. For the three commercial membranes, the mean pore size may be assumed as uniform pore size for the entire membrane to predict the water vapor permeability of the membranes and the mean pore size can be obtained from the wet/dry flow method or from the gas permeation test. However, special care must be taken into account when one uses other membranes, especially laboratory made membranes, with broader pore size distributions than the commercial membranes used in this study.

## 5.  Conclusions

Three types of microporous hydrophobic membranes, polyvinylidene fluoride (GVHP and HVHP) and polytetrafluoroethylene (TF200), were characterized and applied in direct contact membrane distillation, DCMD, processes. The mean pore size and the pore size distribution were determined. The mass transport for the three membranes lies in the transition region and the molecular diffusion is the predominant. The Knudsen contribution to mass transport was insignificant.

The flux increases exponentially with the mean temperature and is higher for the membrane TF200. This was attributed to the high effective porosity of this membrane.

The water vapor permeability obtained from the semi-empirical model (Method 2) increases with temperature and is higher than that obtained from method 1. The later method (Method 1) can not be applied to determine the water vapor permeability of the membranes as an unique value is obtained for each membrane for all range of mean temperatures.

A theoretical model that considers the pore size distribution of the membranes was developed. It was found that the predicted water vapor permeability also increases with temperature and is higher for the membrane TF200 than for the PVDF membranes.

DCMD water vapor permeability calculated by considering the pore size distribution is slightly higher than that obtained assuming a mean pore size for the whole membrane. This was attributed to the low values of the geometric standard deviation of the commercial membranes used, which were found to be near unity. For membranes with higher geometric standard deviations, a large discrepancy is found between the predicted membrane water vapor permeability considering the pore size distribution and the predicted one from the mean pore size. Therefore, care must be taken when one uses the mean pore size instead of the pore size distribution to predict the permeability of porous membranes.

## Acknowledgements

## Nomenclature

*Symbols*

| | |
|---|---|
| $B_w^m$ | water vapor permeability (kg m$^{-2}$ s$^{-1}$ Pa$^{-1}$) |
| $D$ | water diffusion coefficient (m$^2$/s) |
| $d_p$ | pore size (nm) |
| $F$ | DCMD flux (kg/m$^2$ s) |
| $f_i$ | fraction of pores of diameter $d_i$ |
| $g$ | function defined in Eqs. (1) and (2) |
| $G$ | parameters defined in Eqs. (16) and (17) |
| $h$ | heat transfer coefficient (W m$^{-2}$ K$^{-1}$) |
| $J$ | gas permeation velocity (m/s) |
| $K$ | normalization factor in Eq. (3) |
| $Kn$ | Knudsen number |
| $k$ | thermal conductivity (W m$^{-1}$ K$^{-1}$) |
| $k_B$ | Boltzman constant (J/K) |

| $L_p$ | effective pore length (m) |
|---|---|
| $LEPw$ | liquid entry pressure of water (bar) |
| $M_w$ | molecular weight of water (kg/kmol) |
| $N$ | number of pores per unit membrane area |
| $n$ | cumulative number of pores |
| $Nu$ | Nusselt number |
| $P$ | total pressure (Pa) |
| $\bar{p}$ | mean pressure (Pa) |
| $p$ | vapor pressure (Pa) |
| $p_a$ | air pressure (Pa) |
| $Pr$ | Prandtl number |
| $R$ | gas constant (J/mol K) |
| $r$ | pore radius (nm) |
| $Re$ | Reynolds number |
| $T$ | absolute temperature (K) |

*Greek letters*

| $\delta$ | membrane thickness (μm) |
|---|---|
| $\varepsilon$ | void volume |
| $\varepsilon_s$ | surface porosity defined in Eq. (7) |
| $\varepsilon/L_p$ | effective porosity ($m^{-1}$) |
| $\lambda$ | mean free path (nm) |
| $\mu$ | water dynamic viscosity (kg/m.s) |
| $\mu_p$ | mean pore size of the membrane (nm) |
| $\sigma_p$ | geometric standard deviation of pore size distribution |
| $\sigma_w$ | collision diameter of water vapor (Å) |
| $\tau$ | pore tortuosity |
| $\Delta H_v$ | heat of vaporization (kJ/mol) |
| $\Delta P$ | transmembrane pressure (Pa) |

*Subscripts*

| $D$ | diffusion |
|---|---|
| $d$ | dried membrane |
| $f$ | feed |
| $g$ | gas |
| $k$ | Knudsen |
| $m$ | membrane |
| $max$ | maximum pore size |
| $p$ | permeate or pore |
| $s$ | polymer or solid |
| $t$ | transition |
| $w$ | wetted membrane, mean, water |

*Superscripts*

| $C$ | transition |
|---|---|
| $D$ | diffusion |

*K*      Knudsen
*m*      membrane

## References

[1] Lawson, K.W., Lloyd, D.R., Review: Membrane Distillation, J. Membr. Sci., 124 (1997) 1.

[2] Khayet, M., Godino, M.P., Mengual, J.I., Nature of Flow on Sweeping Gas Membrane Distillation, J. Membr. Sci., 170 (2000) 243.

[3] Bandini, S., Saavedra, A., Sarti, G.C., Vacuum Membrane Distillation: Experiments and Modeling, AIChE J., 43-2 (1997) 398.

[4] Izquierdo-Gil, M.A., García-Payo, M.C., Fernández-Pineda, C., Air Gap Membrane Distillation for Sucrose Aqueous Solutions, J. Membr. Sci., 155 (1999) 291.

[5] Khayet, M., Godino, M.P., Mengual, J.I., Modelling Transport Mechanism Through a Porous Partition, J. Non-Equilb. Thermodyn., 26 (2001) 1.

[6] Laganà, F., Barbieri, G., Drioli, E., Direct Contact Membrane Distillation: Modelling and Concentration Experiments, J. Membr. Sci., 166 (2000) 1.

[7] Phattaranawik, J., Jiraratananon, R., Fane, A.G., Effect of Pore Size Distribution and Air flux on Mass Transport in Direct Contact Membrane Distillation, J. Membr. Sci., 215 (2003) 75.

[8] Khayet, M., Matsuura, T., Preparation and Characterization of Polyvinylidene Fluoride Membranes for Membrane Distillation, Ind. Eng. Chem. Res., 40 (2001) 5710.

[9] Kesting, R.E., Synthetic Polymeric Membranes, 2nd edition, John Wiley & Sons, New York, 1985.

[10] Khayet, M., Feng, C.Y., Matsuura, T., Morphological Study of Fluorinated Asymmetric Polyetherimide Ultrafiltration Membranes by Surface Modifying Macromolecules, J. Membr. Sci., 213 (2003) 159.

[11] Kast, W., Hohenthanner, C.R., Mass Transfer Within the Gas Phase of Porous Media, Int. J. Heat & Mass Transfer, 43 (2000) 807.

[12] Matsuura, T., Synthetic Membranes and Membrane Separation Processes, CRC Press, Boca Raton, FL, 1993.

[13] Schofield, R.W., Fane, A.G., Fell, C.J.D., Heat and Mass Transfer in Membrane Distillation, J. Membr. Sci., 33 (1987) 299.

[14] Mengual, J.I., Peña, L., Membrane Distillation, Colloid & Interface Sci., 1 (1997) 17.

[15] Perry, J.H., Chemical Engineers Handbook, 4th edition, McGraw Hill, New York, 1963.

[16] Speraty, C.A., Physical Constants of Fluoropolymers, Polymer Handbook, 3rd edition, Wiley, New York, 1989.